X-ray Debye-Waller factor measurements of solid ^{3}He and ^{4}He

D. A. Arms,* R. S. Shah,† and R. O. Simmons
Frederick Seitz Materials Research Laboratory and Department of Physics, University of Illinois at Urbana-Champaign, Urbana, Illinois 61801

(Received 2 August 2002; revised manuscript received 14 January 2003; published 24 March 2003)

X-ray synchrotron radiation was used to measure Debye-Waller factors of helium crystals for both ^{3}He and ^{4}He in both hcp and fcc phases. To our knowledge, there are no previous measurements for ^{3}He. The ranges studied for ^{3}He and ^{4}He crystals were 11.52–12.82 and 10.95–12.13 cm^3, respectively, and 11.5–18.2 and 12.0–20.3 K. With small uncertainty, only a Gaussian dependence upon momentum transfer Q was found, and no anisotropy was detected in the hcp phase. Mean square atomic deviations, $\langle u^2\rangle$, and Lindemann ratios were obtained. Large Lindemann ratios confirm that these solids are highly anharmonic. The $\langle u^2\rangle$ values agree within an average 1% with computations of Draeger and Ceperley from path integral Monte Carlo methods including unusual extrapolations to the thermodynamic limit. Because the path-integral Monte Carlo (PIMC) computations exhibit a T^3 dependence for $\langle u^2\rangle$, which also depends upon molar volume, an empirical analysis was made of the present data as well as of published x-ray and neutron data on hcp ^{4}He. The volume dependencies are similar to those found from calorimetry, over a large volume range, and the temperature dependencies show similar systematic variations with molar volume both in x-ray data and PIMC results.

DOI: 10.1103/PhysRevB.67.094303 PACS number(s): 67.80.Cx, 67.80.Gb, 61.10.Nz, 63.20.−e

I. INTRODUCTION

A. Atomic vibrations in solid helium

Helium has traditionally been a popular topic of research.[1–3] A noble gas, it is chemically inert and forms a solid through the weak van der Waals force, which is well characterized. Since helium is the second lightest element, the atoms in helium solid have considerable zero-point energy, compared to its cohesive energy. This qualifies it as a ''quantum crystal.'' The large zero-point energy invalidates any harmonic treatment of helium lattice dynamics,[4] and presents a challenge for sophisticated theories and modeling.

One useful measure of the anharmonic nature of a crystal is the mean square deviation of atoms from their average positions, $\langle u^2\rangle$, which usually increases as the crystal temperature increases. A direct determination of $\langle u^2\rangle$ can be made from Debye-Waller measurements. Either neutrons or x rays can be used for ^{4}He, but x rays have the advantage that required sample sizes are much smaller than for neutrons. Because ^{3}He is a very strong absorber of neutrons, x rays are best used when both ^{4}He and ^{3}He are to be studied.

There is an indirect way to arrive at a value for $\langle u^2\rangle$ using measurements of the dispersion of excitations found using coherent inelastic scattering. However, such derived $\langle u^2\rangle$ values can be generated only if a series of assumptions is made. The measurements of well-defined excitations are used to generate a one-phonon density of states, employing a fit to a Born–von Kármán model. The resulting density of states is then used to calculate a value for $\langle u^2\rangle$, neglecting any contributions from ill-defined and/or unusual excitations, commonly seen in solid helium at higher energies. There is enough information from measurements to make such fits for hcp, fcc, and bcc ^{4}He crystals.[5] There are also measurements for hcp ^{3}He crystals,[6] but not enough for a fit. We emphasize that any such value of $\langle u^2\rangle$ generated in this manner neglects the unusual excitations present in helium crystals, unlike the direct $\langle u^2\rangle$ measurements presented here which include all contributions to atomic displacements.

B. Debye-Waller factor

The Debye-Waller factor is an attenuation of coherent scattering, caused by displacements of the atoms from their average positions in the crystal lattice. These displacements are due to both the zero-point energy and the thermal energy in the crystal. The thermal energy decreases with temperature, causing a decrease in attenuation. At zero temperature in helium, only a considerable zero-point motion is left.

The attenuation due to the Debye-Waller factor has the form of

$$I(Q,T)\propto\exp(-2M_Q), \tag{1}$$

where $\mathbf{Q}\equiv\hbar(\mathbf{k}_f-\mathbf{k}_i)$ is the momentum transfer vector of the scattered radiation, and M_Q is the Debye-Waller factor along the direction of $\mathbf{Q}$. The Debye-Waller factor can be expanded as

$$2M_Q=\langle u_Q^2\rangle Q^2-(1/12)(\langle u_Q^4\rangle-3\langle u_Q^2\rangle^2)Q^4+O(Q^6), \tag{2}$$

where $\langle u_Q^2\rangle$ is the (temperature dependent) mean square atomic deviation along the direction of $\mathbf{Q}$. If the deviations of the atoms from their average positions form a Gaussian shape, the Debye-Waller factor can be simplified to its first order term:

$$2M_Q=\langle u_Q^2\rangle Q^2. \tag{3}$$

Solid helium has been shown to have a Gaussian momentum distribution $n(p)$ within small experimental uncertainties using neutron scattering,[7] although this does not necessarily translate to a Gaussian position distribution. Theoretical research claims that, for molar volumes of $V\gtrsim 10$ cm^3, a Gaussian shape for $n(p)$ is not strictly valid.[1] However, up to

 ©2003 The American Physical Society

now, there has been no measurement in crystal helium that shows any deviation from a Gaussian distribution within experimental uncertainty.[8]

With an assumed Gaussian position distribution, Eqs. (1) and (3) result in

$$\ln(I(Q,T)) = -\langle u_Q^2 \rangle Q^2 + \text{const}, \tag{4}$$

showing that if the temperature is fixed and a series of integrated intensity measurements are taken for many elastic peaks (with Q measured for each), $\langle u_Q^2 \rangle$ can be directly measured. This is done by plotting the natural logarithm of the integrated intensities versus Q^2, with the negative of the resulting slope being $\langle u_Q^2 \rangle$ for that particular temperature. The experimental test of this Gaussian assumption is a first object of measurement.

For crystals that can take a cubic basis, such as fcc, any directional dependence of $\langle u_Q^2 \rangle$ must have cubic symmetry. The quadratic contribution to the Debye-Waller factor is necessarily isotropic. For crystals with a hexagonal basis, such as hcp, $\langle u_Q^2 \rangle$ is not isotropic; there are components along the a and c axes: $\langle u_a^2 \rangle$ and $\langle u_c^2 \rangle$. In general, the components for two directions for hcp elemental crystals are not equal, although there is a rough correlation of their ratio to the crystals' lattice parameter c/a ratio. This can be seen in such a comparison using known measurements of $\langle u_a^2 \rangle$ and $\langle u_c^2 \rangle$ for hcp elemental crystals[9] with the corresponding a and c values;[10] the only caveat is that this comparison contains only metals. The lattice spacings a and c were measured for the hcp helium crystals used for this experiment, with an average value of 1.6310(5) for c/a. This value is close to, but clearly somewhat less than, the ideal ratio of $\sqrt{8/3} = 1.6330\ldots$, consistent with early inferences from birefringence measurements.[11] The measured c/a corresponds to a metallic $\langle u_c^2 \rangle / \langle u_a^2 \rangle$ ratio near 1.2. However, helium is an insulator and not a metal, and in the measurements presented here, there is no noticeable difference between $\langle u_a^2 \rangle$ and $\langle u_c^2 \rangle$ for any set of measurements. Because of this, $\langle u_Q^2 \rangle$ is assumed to be isotropic for hcp He, although it is possible there is some currently unmeasured difference between the two components.

From here on, $\langle u_Q^2 \rangle$ will be referred to as simply $\langle u^2 \rangle$, due to isotropy, seen within currently very small limits. In some works, $\langle u^2 \rangle$ refers to the three-dimensional (radial) mean squared atomic deviation (represented here as $\langle u_r^2 \rangle$), whereas here it is the one-dimensional version. For an isotropic distribution, there is a simple relation between the two:

$$\langle u_r^2 \rangle = 3 \langle u^2 \rangle. \tag{5}$$

Since $\langle u^2 \rangle$ is a measure of the energy due to atomic motions present in a crystal, it is interesting to measure the temperature dependence of $\langle u^2 \rangle$, especially at a constant molar volume V. This can be done by taking sets of integrated measurements of elastic peaks as described earlier, each at a different temperature. This process can be very slow, and a quicker way is preferable. If the atomic volume of the crystal can be kept constant during a change in temperature (in order to keep Q constant for an elastic peak), differentiating Eq. (4) with respect to temperature leads to

$$\frac{d}{dT} \langle u^2 \rangle = -\frac{1}{Q^2} \frac{d}{dT} \ln[I(Q,T)]. \tag{6}$$

This shows that the change in mean square atomic deviation, $\Delta \langle u^2 \rangle$, can be found from integrated intensity measurements taken at an elastic peak for small temperature steps ΔT, according to

$$\Delta \langle u^2 \rangle \approx Q^{-2} \Delta \ln[I(Q,T)]. \tag{7}$$

This process only gives a change in $\langle u^2 \rangle$, so the absolute $\langle u^2 \rangle$ needs to be known at one of the points for reference, measured by the previously described method. It is also preferable to use an elastic peak with a relatively high Q for these temperature dependent measurements, as the relative change in integrated intensity is larger at larger Q. If, at some future time, experimental observations reveal a non-Gaussian behavior, this kind of analysis can be modified appropriately.

For clarification of the later discussion, the type of measurements involving many elastic peaks at one temperature will be referred to as Q-dependent measurements, while those of a single peak at different temperatures will be referred to as T-dependent measurements.

II. EXPERIMENTAL DETAILS

A. Helium crystal matters

Growing and manipulating helium crystals precisely requires extensive care, including sensitive thermometry and precise pressure gauges. A full account of the equipment and procedures as used for these measurements was described elsewhere,[12,13] as was the Be pressure cell.[14]

Figure 1 shows the sample arrangements inside the closed cycle refrigerator (CCR), with the cell center orientable on a standard synchrotron beamline goniometer. Because the sintered beryllium used for the sample cell and the outer radiation shield is made from a fine powder, the Debye-Scherrer rings are very uniform, making a highly reproducible background. Calibrated Si diode sensors provided accurate measurements and control of temperature, T, typically to ± 0.01 K. The heater on the fill line can actually be used to melt and grow a crystal more precisely than using the main cryostat heater.

Pressure in the external gas-handling system is generated by an air-driven two-stage diaphragm compressor, to preserve the 99.9999% purity of the sample gases. Absolute pressures were measured by a high-precision Bourdon gauge of small volume, supplemented by a strain gauge cell (sensitive to ± 10 kPa) used to monitor pressure changes during crystal growth and x-ray measurements.

The available ranges of P and T for making measurements were limited, as shown in Fig. 2, by the CCR, by the pressure system, and by the helium phase diagrams. Within these ranges, both fcc and hcp phases of both ^{3}He and ^{4}He are

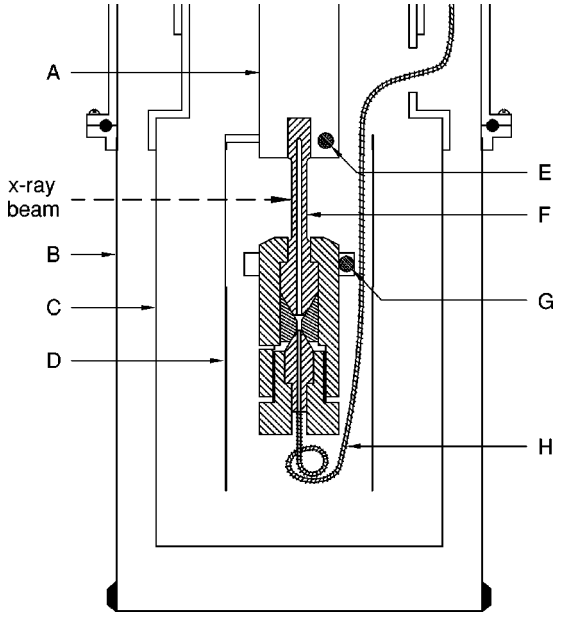

FIG. 1. Internal diagram of the cryostat. (A) OFHC Cu Cold finger extension of CCR and sample cell mount. (B) Lexan vacuum can and containment vessel. (C) Be radiation shield. (D) OFHC Cu radiation shield with aluminized Mylar window. (E) Cold finger temperature sensor. (F) Sintered Be sample cell, 0.8 mm I.D. (G) Sample cell temperature sensor. (H) Sample gas fill line, wrapped with a heater line, attached to cell by maraging steel fitting.

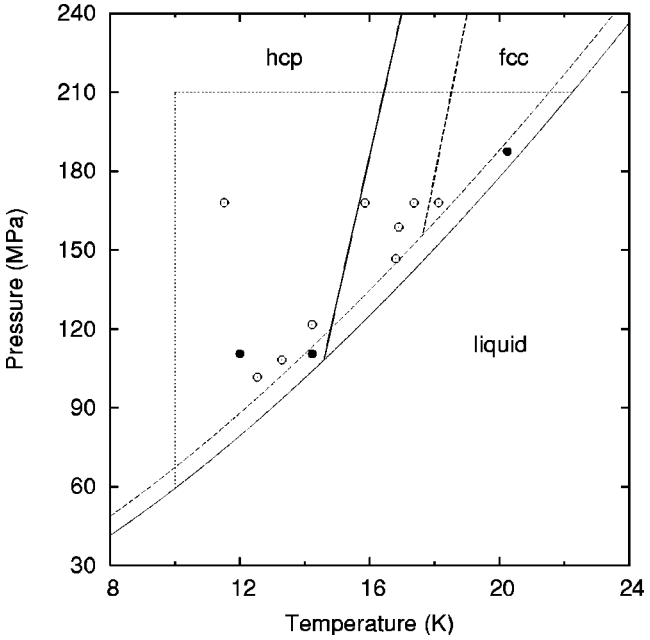

FIG. 2. Phase diagrams of ^{3}He and ^{4}He, with locations of present measurements. The dashed lines and hollow circles correspond to ^{3}He, while the solid lines and filled circles correspond to ^{4}He. The dotted lines delimit the region available for measurements, due to experimental constraints. Both fcc and hcp phases were studied.

available for study. Any temperature dependent measurements to be made have to contend with the narrow temperature range for each phase.

B. X-ray matters

The measurements were done using x-ray synchrotron radiation from bending magnet lines. The photon energy used was 16.00 keV, chosen such that the highest order reflections expected to be visible above background would be at $2\theta = 90°$. The majority of the data presented here was taken at beamline X-14A[15] of the National Synchrotron Light Source (NSLS) at Brookhaven National Laboratory, while the remainder was taken at beamline 1BM-C[16] of the Advanced Photon Source (APS) at Argonne National Laboratory. The x-ray beam at the sample position was horizontally polarized, and had a spot size of 2 mm horizontal by 1 mm vertical at the NSLS and 0.2 mm square at the APS. The choice of spot size is not a simple one, as a small beam will more likely hit a single crystal, but also needs to be stable in position or there will be variations in the amount of illuminated sample due to the cylindrical nature of the sample cell.

Care was taken to measure accurately the integrated intensity values for the reflections. For each reflection, a raw integrated intensity measurement was made by taking a rocking curve of the elastic peak. The individual data counts were corrected for the dead time of the detector (independently measured) and normalized to the incident flux monitor. The detector used at the NSLS was a xenon-filled proportional counter, while at the APS a NaI scintillation counter was used. Since background scans for all the measurements had no nonlinear features, the background for a data scan was simply removed by fitting a line through the background levels on both sides of the peak and subtracting the area under the line; the angular ranges of the scans were wide enough to capture the entire peak. The corrected data for the elastic peak were then numerically integrated.

Additional adjustments to the integrated intensity were done to take into account attenuators and the change of the illuminated volume of the crystal used. Attenuators were placed in the beam between the incident flux monitor and the sample, since the dynamic range of the detectors were not sufficient to measure the high count rates of the lower Q peaks as well as the low counts rates of the higher Q peaks (up to a factor of 10^6 difference). The absorptions of the attenuators were precisely measured at the end of the experiments using the same x-ray beam as the measurements. The need for a volume change correction comes from the changing angle of the sample cell with respect to the x-ray beam, creating a changing path length through the sample and resulting in a changing amount of atoms available for scattering. This effect does not seem to noticeably affect results for a broad beam, since the helium crystals are usually smaller than the size of the beam, making the volume of illuminated crystal rather constant on rotation. For a beam smaller than the normal helium crystal size, the effect is more evident and more in need of correction. Corrections for both cases of beam size were determined, and in practice only the small beam correction was made for the corresponding measurements.

Corrections were also made for the Lorentz factor of $[\sin(2\theta)]^{-1}$ for horizontally polarized photons and for both

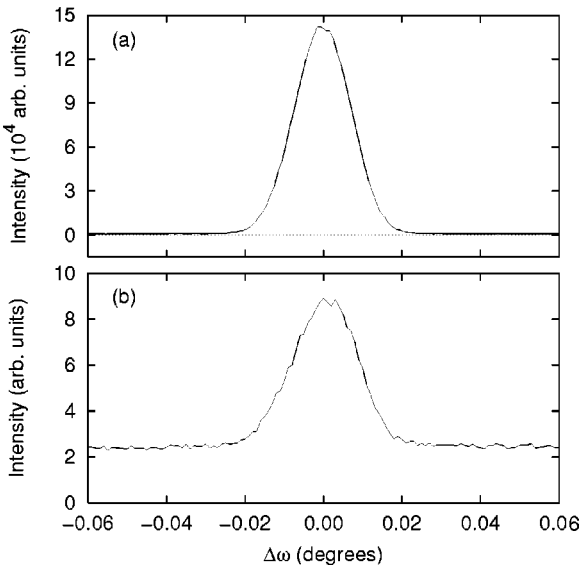

FIG. 3. Rocking curve measurements of an ideal fcc ^{3}He crystal. Shown are the (a) (1 1 1) and (b) (3 3 3) peaks. The only corrections made to the data shown are for dead time and incident flux normalization. The absolute intensities of the scans are normalized with respect to each other, showing the 2×10^4 dynamic range needed for the measurements. The scans are from measurement 3 of Table I.

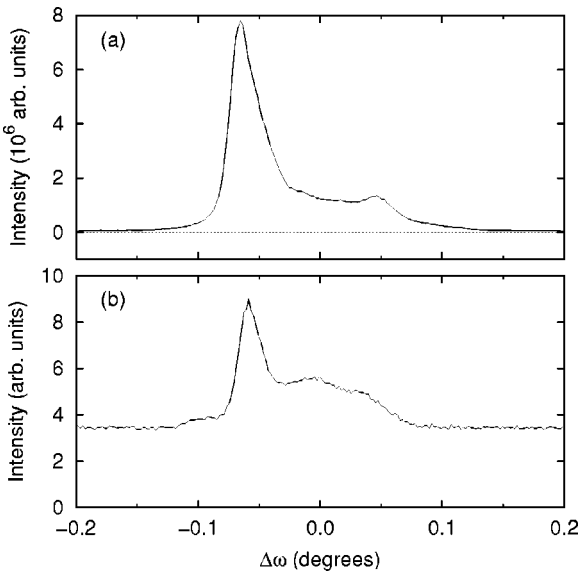

FIG. 4. Rocking curve measurements of typical hcp ^{3}He crystal. Shown are the (a) (0 0 2) and (b) (1 0 7) peaks. The only corrections made to the data shown are for dead time and incident flux normalization. The absolute intensities of the scans are normalized with respect to each other, showing the 10^6 dynamic range needed for the measurements. The scans are from measurement 6 of Table I.

the crystal structure factor of the reflection and the atomic form factor, for which the values used were from Su and Coppens.[17] An additional adjustment could have been made for the contribution due to thermal diffuse scattering (TDS), but TDS effects for measurements taken at synchrotrons are normally small and in practice were made to be insignificant.[18] After all these adjustments were made, the resulting integrated intensity value was used with others from different reflections for determining $\langle u^2\rangle$.

Much effort is required to determine whether the quality of a helium crystal is sufficient for precise integrated intensity measurement. A perfect single crystal filling the entire sample cell is an unrealistic expectation, and there is no need for that degree of quality. Multiple crystals within the x-ray cross section of the sample cell are fine as long as a large, stable, single crystal can be picked out and oriented. The crystals used had mosaic widths at the rocking curve base of no more than 0.25°, with the exception of one which had rocking curve widths of 0.50°, easily seen to be from mosaic by the several peaks in the rocking curve. Examples of rocking curves from both ideal and typical specimen crystals are in Figs. 3 and 4, respectively. For each figure, high Q and low Q reflections are shown, with the full extent of the scans not shown. Note that in each example a very wide range of integrated intensity is covered. The small residual background levels are most easily seen in the high Q scans.

We found what appeared to be a peak at the forbidden (1 1 1) reflection for a hcp crystal at the NSLS, but did not do a strict verification at the time to eliminate the possibility that it arose from multiple scattering. A subsequent long search was made at the APS using another hcp crystal, looking for {1 1 1}, {0 0 1}, and {0 0 3} type peaks, but none of those types were found. This lack of such peaks, forbidden in the hcp structure, confirms that structure and in addition verifies the crystal quality (absence of significant stacking faults).

Ideally, T-dependent measurements would hold the molar volume of the sample constant. However, due to safety concerns, we could not physically isolate the helium in the sample cell from the rest of the pressure system. There is some isolation due to a frozen helium blockage of the fill line. From measured lattice parameter values, it seems the blockage would slip occasionally when the temperature was changed; this was most likely due to changing pressure in the small gas ballast as more solid formed. The T-dependent measurements are affected by this, but the actual effect is very small and not accurately measurable.

III. RESULTS

A. Q-dependent data

There were 13 sets of Q-dependent measurements taken, as shown in Table I. A full listing of the integrated intensity data is available elsewhere.[12] Molar volume values V are derived from lattice parameter measurements. Measurements 6 and 9 were taken at the APS, while the rest were taken at the NSLS.

For each set, the corrected integrated intensity and Q values for every reflection are used to solve for $\langle u^2\rangle$, according to Eq. (4). Examples of such sets are in Figs. 5 and 6. Figure 5 shows measurement 6, which has the largest total number of reflections utilized (all labeled), as well as having reflections with the largest Q values; the rocking curves in Fig. 4 are from this set. Plot (a) from Fig. 6 shows the temperature dependence of $\langle u^2\rangle$ from measurements 13 and 12, as the

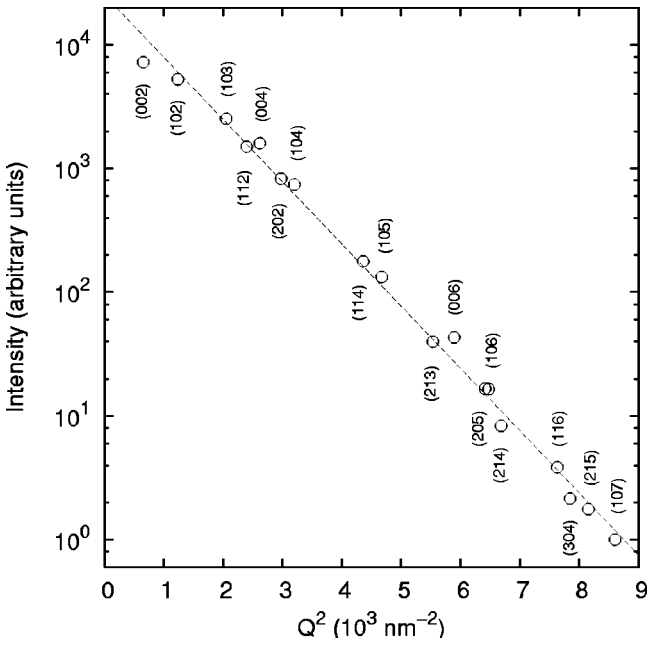

FIG. 5. Debye-Waller measurement of hcp ^{3}He crystal. This is from measurement 6 on Table I. The indices ($h\,k\,l$) of each reflection are shown. Intensities are relative to the smallest intensity value shown.

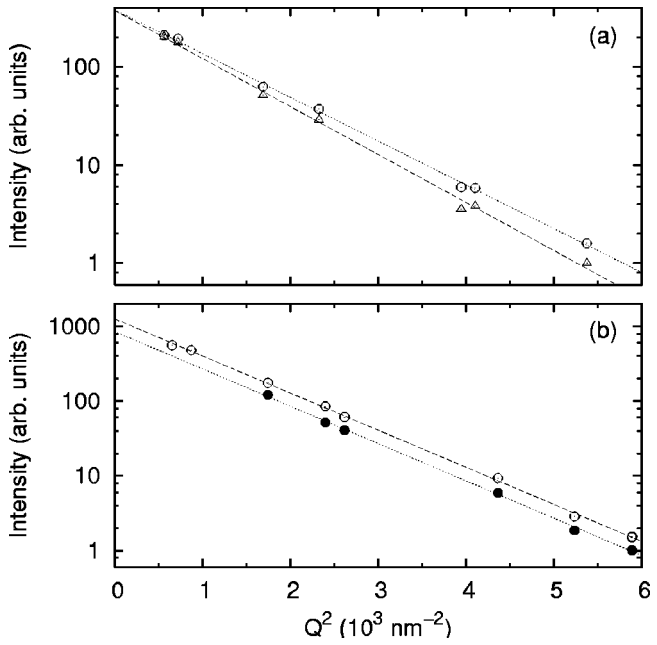

FIG. 6. Debye-Waller measurements from Table I. Intensities are relative to the smallest intensity value shown. Plot (a) is of an hcp ^{4}He crystal at different temperatures, with the circles and triangles corresponding respectively to measurements 13 at 12.00 K, and 12 at 14.23 K; the increase in temperature results in a steeper slope. Plot (b) is of two similar measurements for a fcc ^{3}He crystal at the same temperature, 18.13 K, with the hollow and filled circles corresponding to measurements 3 and 4, respectively. Measurement 3 is multiplied by 1.5 to give a visible offset.

absolute magnitude of the slope increases with a T increase from 12.00 to 14.23 K, as expected. The two data sets are plotted with the same y intercept to illustrate the relative intensity change for each peak. Plot (b) from Fig. 6 shows measurements 3 and 4. The measurements are from the same crystal and the same temperature, demonstrating the reproducibility of the measurements; the rocking curves in Fig. 3 are from one of these sets.

The Lindemann ratio, using Eq. (5), is

$$\text{L.R.} \equiv \frac{\sqrt{\langle u_r^2 \rangle}}{d} = \frac{\sqrt{3\,\langle u^2 \rangle}}{d}, \tag{8}$$

where d is the nearest neighbor distance from lattice parameter measurements. Most materials melt before reaching the present high values, indicative of helium's strong quantum solid nature. The Lindemann ratios in Table I for the hcp crystals generally increase with increasing T or larger V, and the ratios for hcp and fcc tend to be larger for ^{3}He than for ^{4}He. Measurements 8 and 12 are of ^{3}He and ^{4}He, respectively, at 14.23 K, with the ^{3}He molar volume only 2.0%

TABLE I. Q-dependent measurement conditions and data.

Meas. label	Crystal type	Num. of reflections	V (cm^3)	T (K)	$\langle u^2 \rangle$ (10^{-4} nm^2)	$\sqrt{3\langle u^2 \rangle}/d$	Θ_M (K)
1	hcp ^{3}He	7	11.566(3)	15.86(1)	11.55(23)	0.1957(19)	117.1(1.9)
2	hcp ^{3}He	7	11.568(3)	17.37(1)	12.19(66)	0.2011(54)	114.2(4.9)
3	fcc ^{3}He	9	11.578(3)	18.13(1)	11.43(11)	0.1947(09)	121.1(0.9)
4	fcc ^{3}He	7	11.578(3)	18.13(1)	11.50(15)	0.1954(13)	120.5(1.3)
5	hcp ^{3}He	11	11.602(3)	11.52(1)	11.35(22)	0.1938(19)	113.6(1.9)
6	hcp ^{3}He	18	11.607(4)	16.90(1)	11.58(22)	0.1957(19)	118.2(1.8)
7	hcp ^{3}He	11	11.898(3)	16.81(1)	11.96(26)	0.1973(21)	115.0(2.0)
8	hcp ^{3}He	11	12.365(3)	14.23(1)	12.91(41)	0.2023(32)	104.8(2.7)
9	hcp ^{3}He	3	12.526(4)	13.30(1)	13.02(58)	0.2023(45)	103.0(3.8)
10	hcp ^{3}He	4	12.817(3)	12.54(1)	13.43(27)	0.2040(21)	99.3(1.7)
11	fcc ^{4}He	10	10.951(3)	20.25(1)	9.99(27)	0.1855(25)	110.7(2.3)
12	hcp ^{4}He	7	12.120(3)	14.23(1)	11.25(28)	0.1902(24)	93.2(1.9)
13	hcp ^{4}He	7	12.129(3)	12.00(1)	10.26(17)	0.1817(15)	97.5(1.3)

larger than the ^{4}He molar volume; the measured Lindemann ratio for ^{3}He is 6.2% greater than that of ^{4}He. If the ^{3}He measurements 6 and 7 are used as a guide for volume differences, the 2.0% molar volume difference should account for about 1%, making the Lindemann ratio for ^{3}He about 5% larger than for ^{4}He near 12 cm^3 and 14 K, due to ^{3}He atoms having less mass.

It is obvious that $\langle u^2 \rangle$ values are very temperature dependent, but a representation that is relatively insensitive to temperature is very useful, as it lends itself more easily to some type of scaling. For this purpose, $\langle u^2 \rangle$ values have traditionally been converted into equivalent Debye temperatures (of the Debye-Waller type) Θ_M, according to the formula

$$\langle u^2 \rangle = \frac{3\hbar^2 T^2}{m k_B \Theta_M^3} \left[\frac{\Theta_M^2}{4T^2} + \int_0^{(\Theta_M/T)} \frac{\epsilon d\epsilon}{e^\epsilon - 1} \right], \tag{9}$$

which depends on $\langle u^2 \rangle$, the temperature T, and atomic mass m (where m is 3.0160293 amu for ^{3}He or 4.0026032 amu for ^{4}He). The Debye temperature is part of the simplistic (and unrealistic) Debye model, proportional to its maximum frequency. Heat capacity measurements are also converted into their type of equivalent Debye characteristic temperature, Θ_{C_V}, for similar reasons.[4] Values of Θ_M do not have an intrinsic physical meaning, as they depend on a model that is wrong, but they are useful for comparing data from other measurements. For our measurements, values of Θ_M are shown in Table I.

B. *T*-dependent data

Two sets of *T*-dependent measurements were taken. As explained in Sec. II B, these data are not strictly isochoric, but the possible effects of any slight change in molar volume have not been corrected. The hcp ^{3}He set uses the (3 0 0) peak from the crystal used for the *Q*-dependent measurement 5. The $\langle u^2 \rangle$ value for measurement 5 is used as the reference. This set of measurements was done twice, while raising and while lowering the temperature, with good repeatability as the two pieces were consistent to within 2% at each point; an average of the values for each temperature has hence been used. The hcp ^{4}He set uses the (2 1 3) peak from the crystal used for measurements 12 and 13. In this case, the measurement 13 value is used for reference, and the measurement 12 value is then available for an independent comparison. This set was taken mostly while raising the temperature, and a jog is visible in it where the temperature controller had a glitch. Reliability checks were then done at two points below the glitch while lowering the temperature; they were again within 2%. The two sets of data can be seen in Fig. 7, as well as the corresponding *Q*-dependent values. As expected, the $\langle u^2 \rangle$ values rise with temperature for both sets of measurements. For the ^{4}He values there is agreement between the *T*-dependent measurements and the *Q*-dependent measurement 12, if the error bars for measurement 13 are used for the *T*-dependent values.

These values can be converted to Θ_M values as before, seen in Fig. 8 where plot (a) is of the ^{3}He measurements, and plot (b) is that of ^{4}He. In both cases, Θ_M decreases with increasing temperature at an essentially constant molar volume. The decrease for ^{4}He is also evident in the *Q*-dependent values as well.

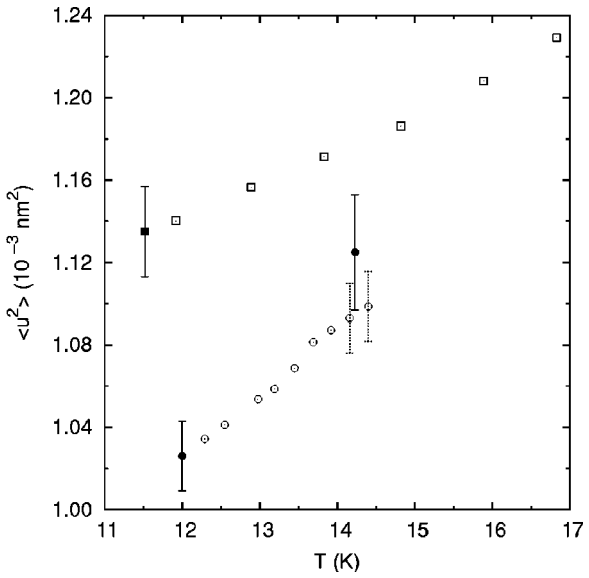

FIG. 7. *T*-dependent Debye-Waller measurements for hcp ^{3}He and hcp ^{4}He. *Q*-dependent measurements (solid points) are used as references for the *T*-dependent measurements (hollow points), since the latter generate $\Delta\langle u^2 \rangle$ values [see Eq. (7)]. The square points are ^{3}He measurements from the crystal used in measurement 5 from Table I, with the (3 0 0) peak measured for the *T*-dependent values. The circle points are ^{4}He measurements from the crystal used in measurements 12 and 13, with the (2 1 3) peak measured for the *T*-dependent values. For the ^{4}He values, measurement 13 (at 12 K) is the reference and 12 is a successful cross-check (where the error bars of measurement 13 are shown with the last two *T*-dependent points). Each isotope has a different molar volume, but both are plotted here for compactness.

IV. DISCUSSION

We first discuss the remarkable agreement of present measured $\langle u^2 \rangle$ values to path-integral Monte Carlo (PIMC) computations over a wide range of experimental conditions. In Sec. IV B, an empirical scaling of data by molar volume is defined in terms of numbers $\langle u^2 \rangle$ and their derivatives, and all published Debye-Waller diffraction data for crystal helium are compared. In Sec. IV C, the dependencies of $\langle u^2 \rangle$ values upon temperature, measured in ^{3}He, are found to be similar, when expressed as Θ_M, to the dependencies upon T of the energies of some excitations in neutron work on ^{4}He. In both cases, such behavior contrasts with that of a quasiharmonic solid. Finally, in Sec. IV D, a variety of other topics are covered, including isotope effects, a search for non-Gaussian contributions to the observed scattering, and a comment on the relation of measurements of atomic kinetic energy. Altogether, it can be seen that the present extensive coverage of conditions of molar volume, of temperature, and of change in isotope now provide a broad coherent outline of these aspects of atomic motion in crystal helium.

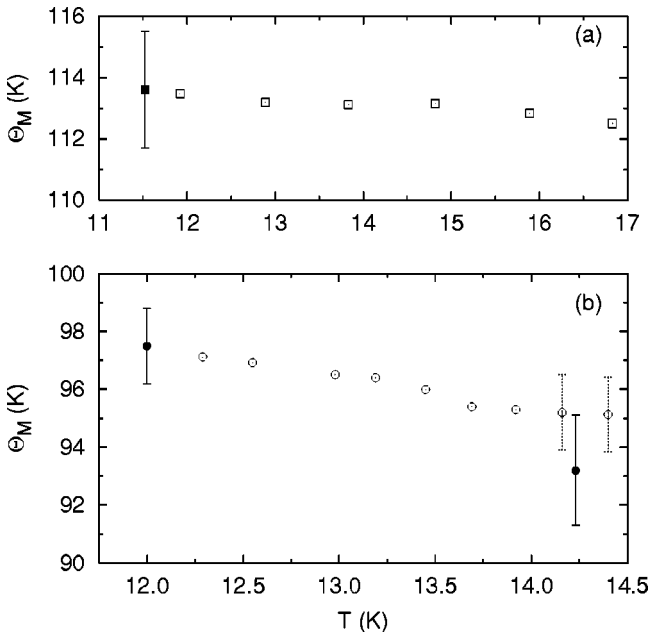

FIG. 8. *T*-dependent Debye-Waller measurements for hcp ^{3}He and hcp ^{4}He, represented as equivalent Θ_M values. Plot (a) corresponds to the ^{3}He measurements shown in Fig. 7, while plot (b) corresponds to the ^{4}He measurements. Note the different *T* ranges for each plot. In both cases, the isochoric Θ_M decreases with increasing *T*.

A. Comparisons to PIMC computations

The present experimental results spurred theoretical work by Draeger and Ceperley regarding the use of PIMC methods for solid helium.[19] Early computations with small PIMC sample sizes produced values of $\langle u^2 \rangle$ consistently about 1/7 lower than present measured values. Further investigation revealed that if the number of atoms, *N*, used for the computational sample size was increased, the resulting $\langle u^2 \rangle$ values rose toward better agreement with experimental values. A method of extrapolating PIMC computations to the thermodynamic limit ($N=\infty$) was thereafter devised, and computations matching the conditions of six of the present measurements were made. The agreement between the experimental and computational values for $\langle u^2 \rangle$ is remarkable in every case, as shown in Table II, where the corresponding experimental values from Table I are also listed.[20]

There are no previous Debye-Waller measurements for ^{3}He, to our knowledge, although there were three previous studies of ^{4}He. The first ^{4}He measurements were done with neutron scattering by Stassis *et al.* for the hcp phase.[21] The others were done with x-ray scattering: Venkataraman made several measurements for the fcc phase,[22] and Burns and Isaacs made a single measurement for the hcp phase at low temperature.[23] Table I of Draeger and Ceperley[19] also shows favorable comparisons to the measurements of Stassis *et al.* and of Venkataraman.

Conversely, there are substantial systematic differences between PIMC results and indirect inferences about $\langle u^2 \rangle$ from inelastic neutron scattering.[5] As noted in Sec. I A, such neutron inferences apparently do not include all contributions to atomic displacements, unlike direct Debye-Waller measurements.

B. Volume scaling of Debye-Waller data

The data presented here, as well as the previous published measurements, are from crystals of varied molar volumes. One may represent them on a common basis, independent of any assumption about the nature of vibrational contributions to $\langle u^2 \rangle$, by volume-dependence of the equivalent number, Θ_M, through a definition of a lumped Grüneisen parameter,

$$\gamma_M = -\frac{\partial \ln \Theta_M}{\partial \ln V}. \tag{10}$$

There are not enough data to provide an experimentally derived γ_M also displaying the possible temperature dependence. In their absence, we note that in helium a fit to γ_{C_V} does exist for Θ_{C_V}, the equivalent Debye temperature for heat capacity measurements. Two different sets of heat capacity measurements at various molar volumes were made for ^{4}He,[24,25] with extrapolations of Θ_{C_V} to $T=0$, resulting in the fit for γ_{C_V} at 0 K:

$$\gamma_{C_V} = 0.8114 + 0.09690\ \ V, \quad 26 \leqslant V(\mathrm{cm}^3) \leqslant 13.7. \tag{11}$$

Less extensive ^{3}He measurements were also taken,[26] and it was shown that ^{3}He tends to conform to the same fit.[24]

In a harmonic analysis, the high and low temperature limits of Θ_{C_V} and Θ_M correspond to certain Debye moments of the distribution, $\omega_D(n)$.[4] Thus, even for a quasiharmonic nonmagnetic insulating solid, Eq. (11) is not ideal for scaling because the low temperature limits correspond to different moments, so that γ_M and γ_{C_V} have different values already

TABLE II. PIMC computations by Draeger and Ceperley (Ref. 19).

Crystal Type	*V* (cm^3)	*T* (K)	$\langle u^2 \rangle$ (10^{-4} nm^2)	Corresponding Measurements	$\langle u^2 \rangle_{exp}$ (10^{-4} nm^2)
fcc ^{3}He	11.54	17.78	11.41(40)	3,4	11.43(11),11.50(15)
hcp ^{3}He	11.90	16.84	11.84(24)	7	11.96(26)
hcp ^{3}He	12.81	12.31	13.26(19)	10	13.43(27)
fcc ^{4}He	10.98	20.00	9.77(39)	11	9.99(27)
hcp ^{4}He	12.12	14.55	11.17(13)	12	11.25(28)
hcp ^{4}He	12.12	11.85	10.24(13)	13	10.26(17)

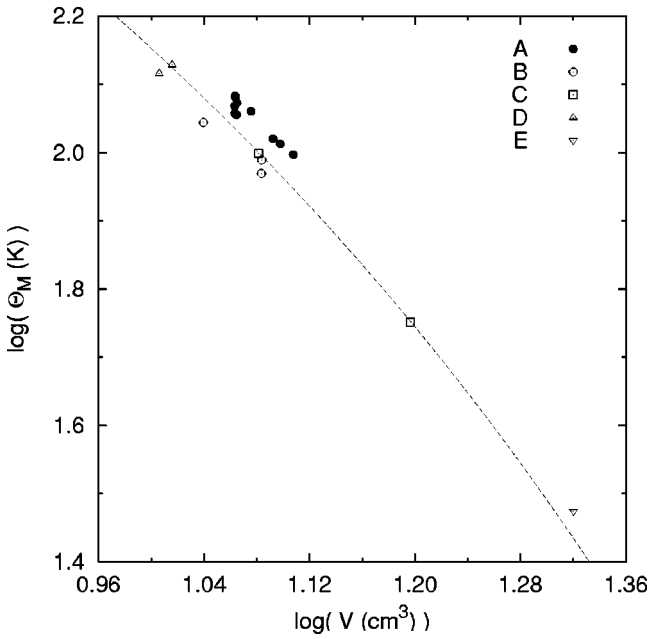

FIG. 9. Current and previous equivalent x-ray Θ_M values at various temperatures. Since the temperatures of each measurement are not the same, this graph is useful only for showing trends. Data set A is the current ^{3}He measurements, while data set B is the current ^{4}He measurements. Data set C is from Stassis *et al.* (Ref. 21) set D is from Venkataraman (Ref. 22) and point E is from Burns and Isaacs (Ref. 23). The dashed line is the Grüneisen parameter fit to heat capacity measurements from Gardner, with the vertical offset set to pass through data set C.

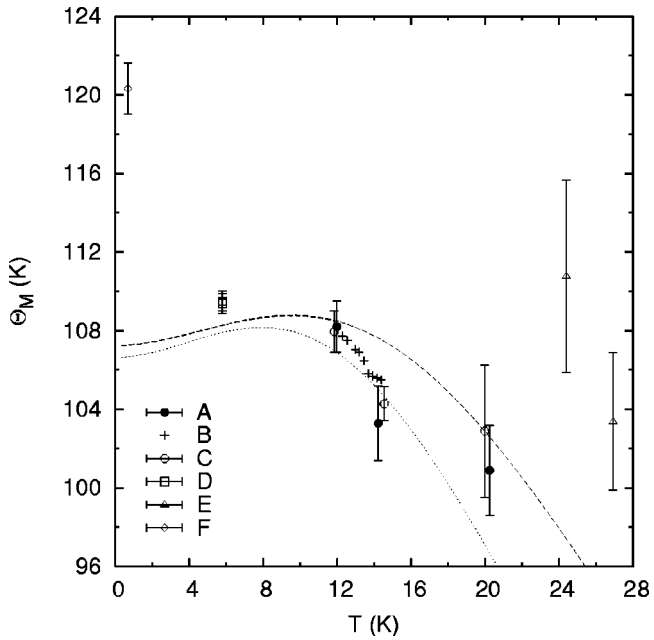

FIG. 10. Graphs of equivalent Θ_M values for ^{4}He measurements and computations, scaled to 11.50 cm^3 using a heat capacity Grüneisen parameter. Data set A is the current *Q*-dependent values, while data set B is the *T*-dependent values. Data set C is the accompanying PIMC computational values generated by Draeger and Ceperley (Ref. 19), with the dashed and dotted curves being the corresponding fits to the computations, corresponding to a 10.98-cm^3 fcc crystal and a 12.12-cm^3 hcp crystal respectively. Data set D is the neutron measurements by Stassis *et al.* (Ref. 21), data set E is x-ray measurements by Venkataraman (Ref. 22), and data point F is by Burns and Isaacs (Ref. 23). Except for the fit curves, all values over 17.5 K correspond to the fcc phase, while all others correspond to the hcp phase. Divergence of the two computational curves at higher *T* is discussed in the text.

in the limiting case. The fact that helium is not a quasiharmonic solid makes the use of this scaling even less reliable. The measured data are also not at $T=0$, which Eq. (11) assumes, although at low temperatures the deviation was seen to be small:[24]

$$\gamma_{C_V}(10\ \mathrm{K})/\gamma_{C_V}(0)\approx 1.02, \quad V=13\ \mathrm{cm}^3. \tag{12}$$

In any case, use of Eq. (11) is instructive purely for qualitative comparison. If the current and previous $\langle u^2\rangle$ measurements, converted to an equivalent Θ_M values, are plotted together versus volume on a log-log scale along with the γ_{C_V} relationship, as in Fig. 9, it can be seen that the ^{3}He and ^{4}He measurements (solid and hollow respectively) roughly follow the relationship. This graph of course displays possible differences arising from temperature differences between the measurements, from structure, and from isotopic mass. We consider those below.

C. Temperature dependences

From computations made at several temperatures, an empirical temperature dependence of

$$\langle u^2\rangle = a + b\,T^3 \tag{13}$$

was found by Draeger and Ceperley, which is used below for comparisons to experimental values. This unexpected cubic dependence was explained by Draeger and Ceperley as arising within a regime of crossover between quantum and classical limits for finite-size scaling of $\langle u^2\rangle$. Note that these computations extended outside the region of the phase diagram accessible by experiment (Fig. 2), being 5–20 K for fcc ^{4}He and 5–18 K for fcc ^{3}He .

Figure 10 shows the present *Q*- and *T*-dependent experimental ^{4}He results converted to Θ_M values scaled to a molar volume of 11.50 cm^3 using Eq. (11). Also shown, similarly scaled, are the values of Stassis *et al.*,[21] Venkataraman,[22] Burns and Isaacs,[23] and the computational ^{4}He Θ_M values from Table II, as well as curves representing fits of the computations to Eq. (13). This graph includes both fcc and hcp measurements, with values over 17.5 K corresponding to the fcc phase and those below 17.5 K corresponding to the hcp phase.

The first thing to be noted about Fig. 10 is that the two curves representing the PIMC fits diverge at higher temperatures. Near 0 K, the scaling seems to be rather good, consistent with the fact that the heat capacity values used for the fit correspond to 0 K, but the fits diverge relatively quickly above 10 K. Since the fits are consistent with the experimental measurements, this implies that the scaling used for this figure is less than ideal, which was expected. Since the

dashed curve is for higher density solid than the dotted curve (10.98 cm^3 versus 12.12 cm^3), the curves corresponding to the even higher density measurements of Venkataraman would have even higher values. Indeed this is consistent with computations by Draeger and Ceperley for the $\langle u^2 \rangle$ values at 24.40 and 25.94 K, which show agreement with her values.

Second, that current isochoric x-ray results are contrary to quasiharmonic behavior can be recognized in another way. If a quasiharmonic fcc crystal is considered, a continuous curve of $\omega_D(n)$ can be composed. For small n it has a positive second derivative, having a minimum for n between 0 and 2; also, there is a larger value for $\omega_D(-2)$ than for $\omega_D(-1)$, making the high temperature limit of Θ_M for that system larger than the low temperature limit.[27] Finally, it is expected that the transition between the two limits should be monotonic, with no local maxima or minima.

This expectation is met in fcc neon, the noble-gas solid closest to helium. From inelastic neutron scattering study, neon's low temperature limit of Θ_M is smaller than the high temperature limit.[28] Magnesium can be used for a comparison to an hcp solid with a c/a ratio close to ideal, and it has limiting cases for Θ_M with the same relationship as neon.[29,30] The Debye moments for neon and magnesium, used to determine the limiting Θ_M values, are derived from the one-phonon density of states obtained from a Born–von Kármán fit to measured phonon dispersion. The same conclusion about the neon frequency moments follows from direct x-ray Debye-Waller measurements on neon by Kabat.[31]

The measurements for helium show a different, decreasing temperature dependence of the present Θ_M. This is clearly shown in Fig. 8 by the T-dependent measurements of both ^{3}He and ^{4}He, as well as in the Q-dependent measurements when looking at the ^{3}He measurements 1 and 2 or at the ^{4}He measurements 12 and 13. Further, the PIMC computations predict this dependence above 10 K, corresponding to the present measurements, seen in Fig. 10 by the curves. Evidence of this dependence was first seen by Venkataraman,[22] who studied helium at smaller molar volumes than those studied in the present work.

The decrease of Θ_M with increasing T shown in Fig. 8 is like the sign and percent shift of the decreases in energy of selected excitation energies seen in neutron work at high density.[5] To the extent that Eq. (9) represents some lumped average of individual contributions, there is consistency with the neutron results. However, present direct $\langle u^2 \rangle$ measurements include all contributions to atomic displacements, unlike the selected neutron response peaks. Indeed, the neutron work lacks data at higher energies.

It is interesting to compare, qualitatively, the volume-scaled behavior of the present Θ_M in Fig. 10 with analogous scaled behavior for the heat capacity Θ_{C_V}, shown in Fig. 11 of Ahlers.[24] In both cases, as the molar volume is decreased, the temperature dependence of the characteristic temperature moves in the direction toward that of a quasiharmonic solid. However, in both cases the molar volume around 12 cm^3 is still in an intermediate regime between the most-quantum behavior (above 20 cm^3), and is quasiharmonic. This latter behavior seems beyond observation in helium. At present densities, helium melts at temperatures around one-tenth of the equivalent Θ_M, and at the highest densities so far studied by x rays near melting,[32] still melts at a temperature (400 K) far below the anticipated Θ_M value for that density.

D. Other topics

Previous workers examined helium isotopic dependencies for heat capacity,[26] for Raman scattering,[33] and for phonons.[6,34] For x-rays, our ^{3}He values of Θ_M seem to be roughly 15 K higher than those for ^{4}He. Using a simple mass-scaling factor of $\sqrt{4/3}$ and a frequency scaling $\hbar\omega = k_B\Theta_M$ at the same V, one sees that the ^{3}He and ^{4}He x-ray values are consistent with such scaling.

The work of Draeger and Ceperley assumed an ideal c/a ratio in hcp. In fcc, they found a small anisotropic Q^4 term in the Debye-Waller factor. The present measurements of many reflections from single crystals did not reveal any anisotropy, however, even in the hcp crystals. All data were therefore analyzed on an isotropic basis, as mentioned earlier.

As shown in Eq. (2), there are higher order terms for the Debye-Waller factor, which do not exist for a Gaussian distribution. Draeger and Ceperley predicted a small presence of these higher order terms,[19] leading to a conclusion that the distribution is neither strictly Gaussian nor isotropic. From the appearance of the graphs of our data sets, it is hard to see any definite curvature to any of them. Nevertheless, an attempt was made to look more carefully for a nonzero higher order term, by fitting the data to a quadratic equation in Q^2:

$$\log[I(Q)] = a - b(Q^2) + c(Q^2)^2. \tag{14}$$

The results of the fit did not show any conclusive evidence of a second order term. The resulting values for c were, for the most part, within the associated statistical error, with both positive and negative values appearing (although mostly positive). The absolute values (and their errors) for c tend to be 1/1000 the size of b. If these errors indicate the limits of possible deviations, then those are about 1/6 the size of the spherically averaged kurtosis found by Draeger and Ceperley in the fcc phase. It should be remembered, however, that the data were analyzed using a calculated free-atom form factor,[17] which is the most strongly Q-dependent aspect of the data reduction.

For a quantum solid with a large Lindemann ratio, one might expect the presence of noticeable higher order Q^2 terms in the Debye-Waller factor, since the approximation used in Eq. (4) ordinarily breaks down when the atomic motion is large. However, PIMC computations showed that crystal helium's atomic distribution has a primarily Gaussian nature, with a minute non-Gaussian component. This is confirmed by the present experimental work. Therefore, as far as the Debye-Waller factor is concerned, anharmonicity present in the crystal is masked.

Finally, we note that the previous close agreement of small-sample PIMC computations with precise kinetic energy measurements[7] for helium is due to kinetic energy being a local property of the quantum crystal. As PIMC work is carried to the thermodynamic limit the kinetic energy changes little,[19] unlike $\langle u^2 \rangle$, which is a large-scale property

of a crystal. PIMC computations of small samples put in a periodic array evidently do not establish the same reference lattice for $\langle u^2 \rangle$.

V. CONCLUSIONS

We have taken x-ray Debye-Waller measurements of the previously unmeasured ^{3}He solid as well as ^{4}He solid, in both the fcc and hcp phases and at various molar volumes and temperatures. The resulting $\langle u^2 \rangle$ values agree with path integral Monte Carlo computations corresponding to the experimental conditions for both isotopes within an average 1%. Such an agreement with essentially *a priori* theory, in the necessary thermodynamic limit, is unprecedented for different isotopes over a range of experimental conditions. It demonstrates both computationally and experimentally that previous indirect inferences from neutron inelastic work[5] about $\langle u^2 \rangle$ in solid helium are too low, containing systematic errors of about 15%. The Lindemann ratios for these measurements, around 0.20 for ^{3}He and 0.19 for ^{4}He, are well beyond what is typical for a solid, and also larger than previously deduced from neutron work. Consideration of the temperature dependence of the $\langle u^2 \rangle$ measurements shows that helium at present molar volumes certainly does not exhibit a quasiharmonic behavior.

ACKNOWLEDGMENTS

We especially want to thank C. T. Venkataraman for all her advice and help with the experiment, and we acknowledge useful discussions with E. W. Draeger, D. M. Ceperley, and M. V. Klein. This work was supported by the U.S. Department of Energy, Division of Materials Sciences under Award No. DEFG02-91ER45439 through the Frederick Seitz Materials Research Laboratory at the University of Illinois at Urbana-Champaign. Use of the National Synchrotron Light Source was supported by the U.S. Department of Energy, Division of Materials Sciences and Division of Chemical Sciences, under Contract No. DE-AC02-98CH10886, and use of the Advanced Photon Source was supported by the U. S. Department of Energy, Office of Science, Office of Basic Energy Sciences, under Contract No. W-31-109-Eng-38. At the NSLS we gratefully acknowledge the help of T. Gog, and at the APS the help of G. Srajer, J. Lang, and the rest of SRI-CAT.

*Present address: MHATT-CAT, Advanced Photon Source, Argonne National Laboratory, Argonne, IL 60439. Electronic address: dohnarms@anl.gov

†Present address: Intel Corporation, Hillsboro, Oregon 97124.

[1] H. R. Glyde, *Excitations in Liquid and Solid Helium* (Oxford University, New York, 1994).

[2] E. R. Dobbs, *Solid Helium Three* (Clarendon, Oxford, 1994).

[3] R. O. Simmons, in *Particle Scattering, X-ray Diffraction, and Microstructure of Solids and Liquids*, edited by M. Ristig and K. A. Gernoth (Springer-Verlag, Berlin, 2002).

[4] T. H. K. Barron and G. K. White, *Heat Capacity and Thermal Expansion at Low Temperatures* (Kluwer, New York, 1999), p. 59.

[5] hcp: R. A. Reese, S. K. Sinha, T. O. Brun, and C. R. Tilford, Phys. Rev. A **3**, 1688 (1971); hcp and bcc: V. J. Minkiewicz, T. A. Kitchens, G. Shirane, and E. B. Osgood, *ibid.* **8**, 1513 (1973); fcc: J. Eckert, W. Thomlinson, and G. Shirane, Phys. Rev. B **16**, 1057 (1977); C. Stassis, G. Kline, W. Kamitakahara, and S. K. Sinha, *ibid.* **17**, 1130 (1978); J. Eckert, W. Thomlinson, and G. Shirane, *ibid.* **18**, 3074 (1978).

[6] C. Seyfert, R. O. Simmons, H. Sinn, D. A. Arms, and E. Burkel, J. Phys.: Condens. Matter **11**, 3501 (1999).

[7] R. C. Blasdell, D. M. Ceperley, and R. O. Simmons, Z. Naturforsch. **48a**, 433 (1993).

[8] In normal fluid ^{4}He, it is reported that there are significant deviations: R. T. Azuah, W. G. Stirling, H. R. Glyde, P. E. Sokol, and S. M. Bennington, Phys. Rev. B **51**, 605 (1995).

[9] N. G. Krishna and D. B. Sirdeshmukh, Acta Crystallogr., Sect. A: Found. Crystallogr. **54**, 513 (1998).

[10] W. B. Pearson, *Handbook of Lattice Spacings and Structures of Metals* (Pergamon, New York, 1967), Vol. 2.

[11] J. E. Vos, R. V. Kingma, F. J. Van der Gaag, and B. S. Blaisse, Phys. Lett. **24A**, 738 (1967).

[12] D. A. Arms, Ph.D. thesis, University of Illinois at Urbana-Champaign, 1999.

[13] C. T. Venkataraman and R. O. Simmons, Rev. Sci. Instrum. **67**, 3365 (1996), and CD-ROM.

[14] A. T. Macrander and R. K. Crawford, Phys. Status Solidi A **43**, 611 (1977); A. T. Macrander, Phys. Rev. B **21**, 2549 (1980).

[15] A. Habenschuss, G. E. Ice, C. J. Sparks, and R. A. Neiser, Nucl. Instrum. Methods, Phys. Res. A **266**, 215 (1988).

[16] J. C. Lang, G. Srajer, J. Wang, and P. L. Lee, Rev. Sci. Instrum. **70**, 4457 (1999).

[17] Z. Su and P. Coppens, Acta Crystallogr., Sect. A: Found. Crystallogr. **53**, 749 (1997).

[18] R. Bachmann, H. Kohler, H. Schulz, and H. Weber, Acta Crystallogr., Sect. A: Found. Crystallogr. **41**, 35 (1985).

[19] E. W. Draeger and D. M. Ceperley, Phys. Rev. B **61**, 12 094 (2000).

[20] The molar volume values in Table I differ from those of Draeger and Ceperley (Ref. 19), due to the experimental values having been further refined during full data analysis after the computations were made.

[21] C. Stassis, D. Khatamian, and G. R. Kline, Solid State Commun. **25**, 531 (1978).

[22] C. T. Venkataraman, Ph.D. thesis, University of Illinois at Urbana–Champaign, 1996.

[23] C. A. Burns and E. D. Isaacs, Phys. Rev. B **55**, 5767 (1997).

[24] G. Ahlers, Phys. Rev. A **2**, 1505 (1970).

[25] W. R. Gardner, J. K. Hoffer, and N. E. Phillips, Phys. Rev. A **7**, 1029 (1973).

[26] H. H. Sample and C. A. Swenson, Phys. Rev. **158**, 188 (1967).

[27] T. H. K. Barron, A. J. Leadbetter, J. A. Morrison, and L. S. Salter, Acta Crystallogr. **20**, 125 (1966).

[28] J. A. Leake, W. B. Daniels, J. Skalyo, Jr., B. C. Frazier, and G. Shirane, Phys. Rev. **181**, 1251 (1969).

[29] R. Pynn and G. L. Squires, Proc. R. Soc. London, Ser. A **326**, 347 (1972).

[30] H. R. Schober and P. H. Dederichs, in *Metals: Phonon States*,

Electron States, and Fermi Surfaces, edited by K.-H. Hellwege and J. L. Olsen, Landolt-Börnstein, New Series, Group III, Vol. 13, Pt. a (Springer-Verlag, New York, 1981), p. 84.

[31] F. N. Kabat, Ph.D. thesis, University of Illinois at Urbana-Champaign, 1971.

[32] P. Loubeyre, R. LeToullec, J. P. Pinceaux, H. K. Mao, J. Hu, and R. J. Hemley, Phys. Rev. Lett. **71**, 2272 (1993).

[33] R. E. Slusher and C. M. Surko, Phys. Rev. B **13**, 1086 (1976).

[34] C. Seyfert, Ph.D. thesis, Universität Rostock, 1998.